



A clinical-radiomics nomogram to predict early neurological deterioration in patients with stroke undergoing intravenous thrombolysis

Xiao-Guang Zhang^a, Shan-Shan Jiang^a, Dong Zhang^a, Shu-Hua Chen^a, Yu-Ming Kong^a, Yue-Ying Bai^b, Zhi-Chun Gu^{c,*}, Yun-Hua Yue^{a,*}

^aDepartment of Neurology, Yangpu Hospital, School of Medicine, Tongji University, Shanghai, China; ^bBiology Department, Boston College, Chestnut Hill, Massachusetts, USA; ^cDepartment of Pharmacy, Ren Ji Hospital, Shanghai Jiao Tong University School of Medicine, Shanghai, China

Abstract

Background: Anticipating early neurological deterioration in patients with ischemic stroke undergoing intravenous thrombolysis poses a considerable challenge in clinical practice. This study aimed to develop and validate a diffusion-weighted imaging (DWI)-based clinical-radiomics nomogram for predicting early neurological deterioration in patients with ischemic stroke without large vessel occlusion or hemorrhagic transformation undergoing intravenous thrombolysis.

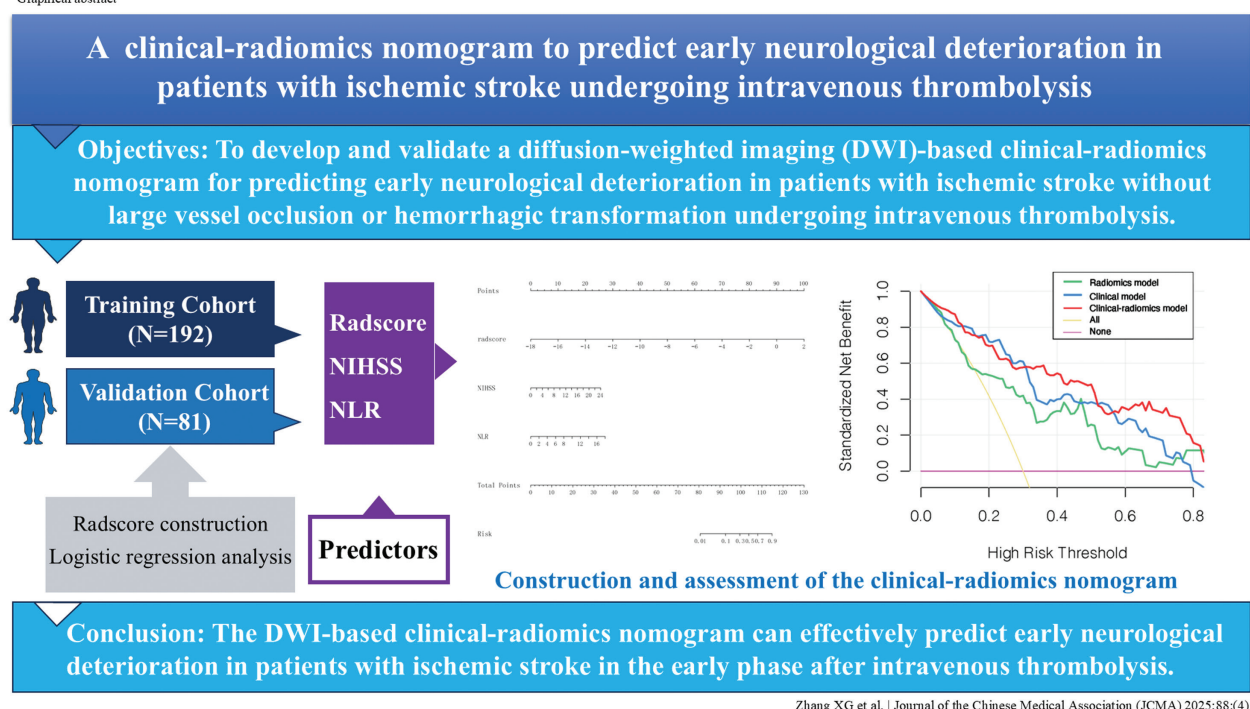
Methods: A total of 273 patients with stroke were randomly divided into training (n = 192) and validation (n = 81) cohorts at a ratio of 7:3. DWI images taken within 24 hours post-intravenous thrombolysis were used to extract radiological features. The *t* test, least absolute shrinkage, and selection operator algorithm were used for feature selection. These features were used to create a radiomics score (radscore) for each patient. Combined with the clinical features, a logistic regression model was used to select independent risk factors that were used to construct a clinical-radiomics nomogram. The performance of the nomogram was evaluated using the area under the curve (AUC), calibration, discrimination, and decision curve analysis.

Results: A total of 1307 radiomics features were extracted from each patient's data. A total of 310 radiomics features were found to be stable after being screened by intraclass correlation coefficients. Seven features were included in the construction of the radscore. The AUC of the clinical-radiomics nomogram was 0.89 (95% CI, 0.83-0.95) in the training cohort and 0.95 (95% CI, 0.90-0.99) in the validation cohort. The calibration curve and decision curve analysis indicated favorable calibration and net clinical benefits of the nomogram.

Conclusion: A DWI-based clinical-radiomics nomogram can effectively predict early neurological deterioration in patients with ischemic stroke in the early phase after intravenous thrombolysis.

Keywords: Diffusion-weighted imaging; Early neurological deterioration; Intravenous thrombolysis; Nomogram; Radiomics

Graphical abstract



1. INTRODUCTION

Ischemic stroke is a leading contributor to disability and death worldwide.¹ The re-establishment of blood flow to the targeted vessel has been established as an efficacious strategy to mitigate the severity of disability and the risk of death in affected individuals. Intravenous administration of recombinant tissue plasminogen activator (rt-PA) for thrombolysis is a cost-effective and pragmatic therapeutic intervention.² Despite these advancements, a substantial number of patients (<50%) achieve a state of functional autonomy, defined by scores of 0 to 2 on the modified Rankin Scale, after a 90-day posttreatment period, thereby exposing the remainder to elevated risks of disability and mortality.³ The phenomenon of early neurological deterioration (END) has been identified as a principal factor contributing to the suboptimal 90-day outcomes in patients with ischemic stroke after intravenous thrombolysis.⁴ END is typically characterized by a four-point escalation in the National Institutes of Health Stroke Scale (NIHSS) starting from the initial assessment up to 24 hours posttreatment.^{4,5} The prevalence of END after thrombolysis is estimated to range between 5% and 40%.⁶ A plethora of variables have been implicated in the genesis of END, but the intrinsic mechanisms remain largely obscure.⁷

In clinical practice, if END occurs within 24 hours post-thrombolysis, a follow-up computed tomography (CT) scan of the brain is typically performed to ascertain whether symptomatic intracranial hemorrhage has occurred. Concurrently, a CT angiography is performed to evaluate the presence of a large vessel occlusion. Nonetheless, aside from these two scenarios, there is a lack of robust clinical predictive approaches for END, attributed to the occlusion of perforating arteries leading to infarction. END is predominantly attributed to the progression of infarction after thrombolysis.⁸ However, it is not meaningful to reassess the expansion of infarct volume using magnetic resonance imaging (MRI) after END manifestation. A prior study has also established that the initial diffusion-weighted imaging (DWI) lesion volume, determined within the initial six-hour window subsequent to the identification of intracranial internal carotid artery or middle cerebral artery occlusion, serves as an indicator of impending END.⁹ This finding provides a valuable basis for predictive models based on initial neuroimaging data. However, the limitations of conventional image evaluation techniques are apparent because they are restricted in their ability to provide comprehensive insights. Therefore, there is an urgent need to develop automatic, reproducible, and quantitative methods capable of effectively assessing the infarct characteristics to predict END following thrombolysis.

Radiomics, a recently developed image-processing technique, exhibits promise in numerous pathologies, including intracranial atherosclerosis, ischemic stroke, intraparenchymal hemorrhage, and glioblastoma, using various imaging modalities.¹⁰⁻¹³ Radiomics surpasses traditional imaging analysis by revealing subtleties, such as the disorder of pixel distribution (entropy) and homogeneity, which are elements that often elude detection

by radiologists.¹³ It provides a more precise quantitative analysis than the standard techniques. Additionally, radiomics facilitates a more nuanced understanding of lesion characteristics, including volume, dimension, form, density, and textural attributes.¹⁰ This capability to extract a comprehensive set of high-dimensional features enables radiomics to forge a correlation between clinical outcomes and imaging findings.¹⁴ The utilization of radiomics techniques for forecasting stroke prognosis is encouraging.^{15,16} However, to the best of our knowledge, no existing study has investigated the application of radiomic profiling to anticipate END after thrombolytic therapy.

The principal aim of this study is the construction and verification of a predictive tool, the nomogram, which integrates a radiomics score (radscore) to estimate the likelihood of END in patients with acute stroke undergoing intravenous thrombolysis.

2. METHODS

2.1. Patients

We conducted a single-center retrospective study using data collected from January 2016 to March 2024 from 273 patients with acute ischemic stroke at the Department of Neurology, Yangpu Hospital, Tongji University School of Medicine. Data collection was approved by the Ethics Committee of the Yangpu Hospital, Tongji University School of Medicine (Ethical Approval Number LL-2023-SCI-002). Informed consent was obtained from all individuals involved. The inclusion criteria were as follows: (1) age >18 years, (2) rt-PA treatment within 4.5 hours of the onset of stroke symptoms, and (3) END (characterized by a four-point escalation on the NIHSS) within the first 24 hours after thrombolysis. Patients were excluded based on the following criteria: (1) MRI examination after 24 hours of thrombolysis, (2) absence of MRI or DWI-negative infarction, (3) large vessel occlusion, (4) END caused by hemorrhagic transformation post-rt-PA, and (5) incomplete baseline data.

Demographic characteristics, vascular risk factors, clinical data, conventional radiological findings, and laboratory data were also collected. The demographic characteristics included age and sex. The vascular risk factors included hypertension, diabetes mellitus, stroke, coronary artery disease, atrial fibrillation, and smoking status. Clinical data included systolic blood pressure, baseline NIHSS score, Trial of ORG 10172 in Acute Stroke Treatment (TOAST) criteria, onset-to-arrival time, door-to-needle time, oral antiplatelet drugs, and statins. Conventional radiological images included the lesion location and watershed infarction. Laboratory data included white blood cell counts; C-reactive protein, fibrinogen, D-dimer, creatinine, urea nitrogen, glucose, cystatin C, homocysteine, triglyceride, total cholesterol, high-density lipoprotein, and low-density lipoprotein levels; and neutrophil-to-lymphocyte (NLR), platelet-to-lymphocyte (PLR), and lymphocyte-to-monocyte ratios. Patients identified with END were screened for an increase of four points on the NIHSS between the initial assessment and 24 hours after treatment. The patients were then randomly divided into training (n = 192, 70%) and validation (n = 81, 30%) cohorts for model construction and evaluation, respectively.

2.2. MRI acquisition

For MR examinations of patients with stroke within 24 hours of receiving intravenous thrombolysis, a 3.0T MR scanner (Magnetom Skyra; Siemens Healthineers AG, Erlangen, Bavaria, Germany) was utilized. The imaging protocol of the Siemens MR system for DWI was specified with the following parameters: repetition time of 4500 milliseconds, echo time of 73 milliseconds, slice thickness of 5 mm with an interslice gap of 0.77 mm, and b values of 0 and 1000 seconds per square millimeter.

*Address correspondence. Prof. Zhi-Chun Gu, Department of Pharmacy, Ren Ji Hospital, Shanghai Jiao Tong University School of Medicine, 1630 East Road, Pudong New Area, Shanghai 200127, China. E-mail address: guzhichun213@163.com (Z.-C. Gu); Prof. Yun-Hua Yue, Department of Neurology, Yangpu Hospital, School of Medicine, Tongji University, 450 Tengguy Road, Yangpu Area, Shanghai 200090, China. E-mail address: Yunhua.Yue@tongji.edu.cn (Y.-H. Yue).

Journal of Chinese Medical Association. (2025) 88: 273-282.
Received July 23, 2024; accepted January 23, 2025.

doi: 10.1097/JCMA.0000000000001213

Copyright © 2025, the Chinese Medical Association. This is an open access article under the CC BY-NC-ND license (<http://creativecommons.org/licenses/by-nc-nd/4.0/>)

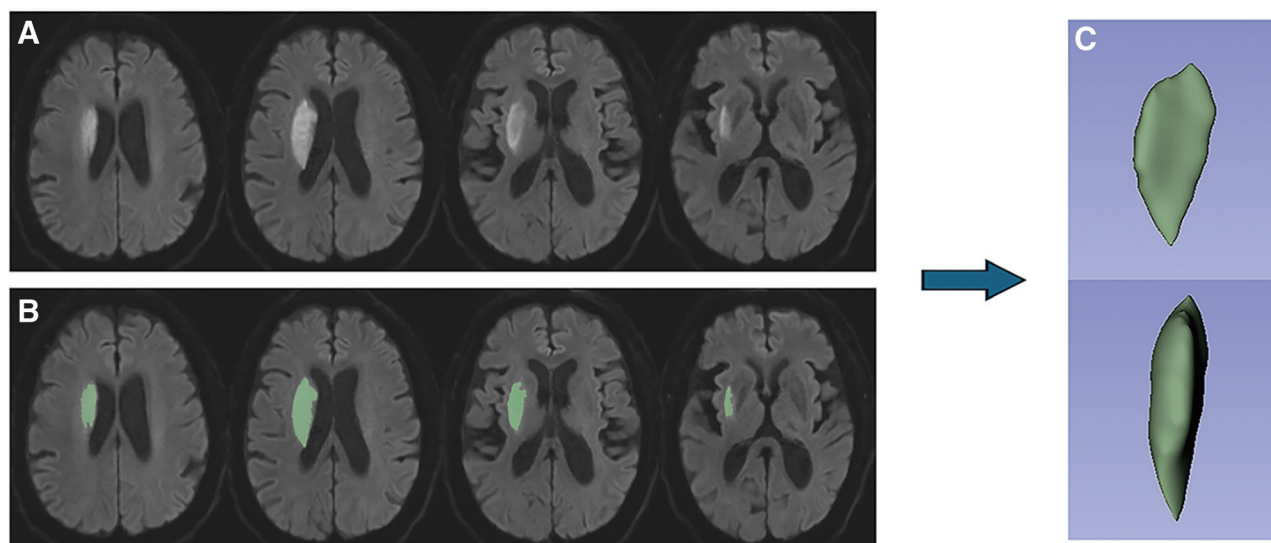


Fig. 1 Delineation of the DWI infarction areas using 3D slicer software. A, Left basal ganglia infarction on DWI. B, The ROI in the area of the left basal ganglia infarction is indicated by the green area. C, 3D ROI for the entire DWI infarction area. DWI = diffusion-weighted imaging; ROI = region of interest.

2.3. Region of interest segmentation and radiomics feature extraction

Segmentation of images was executed by loading Digital Imaging and Communications in Medicine files into 3D Slicer, an open-source medical imaging software platform, version 5.0.3. The Segment Editor tool facilitated manual sequential segmentation.¹⁷ Two experienced neurologists, each with over 5 years of expertise in neuroimaging diagnostics—specifically 6 and 10 years, respectively—delineated all regions of interest (ROIs) on DWI sequences, guided by prominent high-intensity signals (Fig. 1). A subset of 30 lesions was randomly selected to evaluate the reliability of feature extraction. This assessment adhered to established criteria for the selection and reporting of intraclass correlation coefficients (ICCs) in reliability studies.¹⁸

Radiomics feature extraction was conducted using a radiomics module within the 3D Slicer platform. This module interfaces with PyRadiomics, an open-source Python library that facilitates the extraction of radiomic characteristics from medical imaging data. The extracted features were organized into distinct categories, including shape-based descriptors, first-order statistical measures, gray-level co-occurrence matrices (GLCM), gray-level dependence matrices (GLDM), gray-level run-length matrices, gray-level size zone matrices, and neighborhood gray-tone difference matrices. Comprehensive details regarding these radiomics features are available on the PyRadiomics documentation webpage at (<http://pyradiomics.readthedocs.io>).

2.4. Radiomics feature selection

To mitigate the impact of interobserver variability in manual segmentation, ICC was determined for each radiomics feature, prioritizing those that demonstrated high reliability. Subsequently, a *t* test was used to compare the stable features, those with ICCs indicating strong stability, between the patient groups with and without END. Features that exhibited *p* values below the 0.05 threshold in the *t* test were subjected to analysis using the least absolute shrinkage and selection operator (LASSO) regression model. Through the application of 5-fold cross-validation, features that yielded nonzero coefficients were identified and incorporated into the development of the radiomic signature.

2.5. Construction and assessment of the nomogram

The radscore for each participant was computed based on features that had nonzero coefficients in the LASSO regression model. A univariate logistic regression analysis was used to identify the predictors of END for the creation of a predictive nomogram. Subsequently, a multivariate logistic regression analysis was performed, incorporating factors that proved significant in the univariate analysis to formulate the nomogram. Finally, the nomogram, which integrated clinical parameters and the radscore, was crafted using data from the training set and subsequently appraised with the validation set. Model performance was assessed using the area under the curve (AUC) metric for both the training and validation groups. The discrimination of the nomogram model was confirmed using receiver operating characteristic (ROC) curve analysis, with the AUC serving as a quantification measure. The calibration of the model was assessed both graphically through calibration plots and statistically using the Hosmer-Lemeshow test. To further evaluate the clinical utility of the nomogram, decision curve analysis (DCA) was performed. This analysis calculated the net benefit over a range of threshold probabilities for both the training and validation cohorts, providing insights into the practical clinical value of the model.

2.6. Statistical analysis

The *t* test was used to evaluate the disparity in the distribution of initial subject attributes across the two study cohorts. For continuous variables, summaries were presented as median values alongside interquartile ranges. When necessary, the Mann-Whitney *U* test was used for univariate assessments of these variables. Categorical data were depicted in terms of frequency counts and their corresponding percentages, with the chi-square or Fisher's exact test was used to analyze any variations between groups. The Youden index was used to calculate the accuracy, sensitivity, specificity, and positive and negative predictive values (PPV and NPV).¹⁹ Statistical computations were performed using R software (version 4.2.1; www.r-project.org). All statistical tests were two-tailed, with a *p* value of <0.05 set as the threshold for statistical significance.

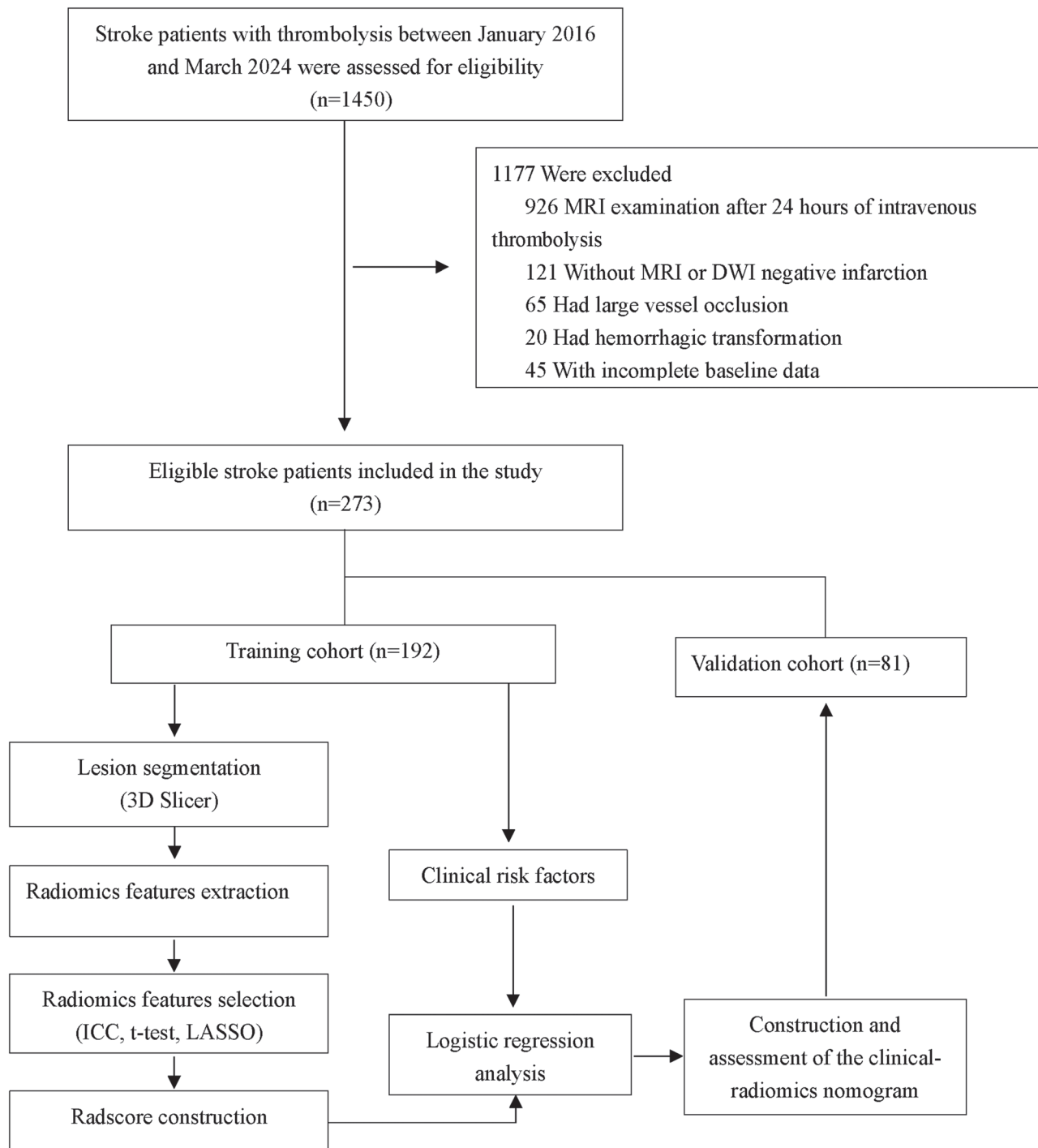


Fig. 2 The workflow of this study. DWI = diffusion-weighted imaging; ICC = intraclass correlation coefficient; LASSO = least absolute shrinkage and selection operator; MRI = magnetic resonance imaging.

3. RESULTS

3.1. Patient summary

From January 2016 to March 2024, 1450 patients with acute ischemic stroke who received intravenous thrombolysis were included. Based on the exclusion criteria, 1177 patients were excluded. Among them, 926 patients underwent MRI examination more than 24 hours after intravenous thrombolysis, 121 patients without MRI or with DWI-negative infarction, 65

patients with large vessel occlusion, 20 patients with hemorrhagic transformation, and 44 patients with incomplete baseline data. Thus, 273 patients were included in our study (192 and 81 in the training and validation cohorts, respectively) (Fig. 2). The demographic and clinical characteristics, conventional radiological imaging, and radscores of the patients in the training and validation cohorts are summarized in Table 1. Except for the NIHSS ($p < 0.001$), TOAST ($p = 0.001$), fibrinogen ($p = 0.005$), NLR ($p < 0.001$), PLR ($p = 0.001$), and radscores ($p <$

Table 1
Baseline characteristics of patients in the training and validation cohorts

Variables	Training cohort (n = 192)	Non-END (n = 166)	END (n = 26)	Validation cohort (n = 81)	<i>p</i> ^a	<i>p</i> ^b
Age	70.00 (62.75, 83.00)	70.00 (62.00, 83.00)	70.00 (64.25, 81.50)	71.00 (63.00, 75.00)	0.968	0.754
Sex, n (%)					0.327	0.378
Male	127 (66.15)	112 (67.47)	15 (57.69)	58 (71.60)		
Female	65 (33.85)	54 (32.53)	11 (42.31)	23 (28.40)		
Hypertension, n (%)	130 (67.71)	112 (67.47)	18 (69.23)	64 (79.01)	0.858	0.060
Diabetes, n (%)	51 (26.56)	43 (25.90)	8 (30.77)	25 (30.86)	0.601	0.469
Stroke, n (%)	45 (23.44)	39 (23.49)	6 (23.08)	21 (25.93)	0.963	0.661
CAD, n (%)	33 (17.19)	31 (18.67)	2 (7.69)	13 (16.05)	0.271	0.818
Atrial fibrillation, n (%)	26 (13.54)	24 (14.46)	2 (7.69)	5 (6.17)	0.529	0.080
Smoking, n (%)	94 (48.96)	79 (47.59)	15 (57.69)	45 (55.56)	0.338	0.319
Systolic blood pressure, n (%)	154.50 (141.00, 172.00)	154.00 (140.00, 170.75)	159.50 (149.25, 176.75)	153.00 (140.00, 171.00)	0.108	0.602
NIHSS	5.00 (3.00, 8.25)	4.00 (3.00, 8.00)	9.00 (8.00, 11.75)	5.00 (3.00, 8.00)	<0.001	0.335
TOAST, n (%)					0.001	0.015
Large-artery atherosclerosis	58 (30.21)	50 (30.12)	8 (30.77)	32 (39.51)		
Cardioembolism	47 (24.48)	33 (19.88)	14 (53.85)	11 (13.58)		
Small-artery occlusion	61 (31.77)	58 (34.94)	3 (11.54)	25 (30.86)		
Other determined etiology	21 (10.94)	21 (12.65)	0 (0.00)	5 (6.17)		
Undetermined etiology	5 (2.60)	4 (2.41)	1 (3.85)	8 (9.88)		
OTA	91.00 (58.75, 143.00)	96.00 (60.25, 144.75)	80.50 (50.50, 121.25)	90.00 (60.00, 134.00)	0.464	0.876
DNT	36.00 (29.00, 45.00)	37.00 (29.00, 45.00)	33.00 (29.00, 38.75)	31.00 (27.00, 36.00)	0.339	0.009
Oral antiplatelet drugs, n (%)	35 (18.23)	32 (19.28)	3 (11.54)	20 (24.69)	0.498	0.224
Statin, n (%)	41 (21.35)	39 (23.49)	2 (7.69)	17 (20.99)	0.068	0.946
Location, n (%)					0.727	0.468
Anterior circulation	124 (64.58)	108 (65.06)	16 (61.54)	56 (69.14)		
Posterior circulation	68 (35.42)	58 (34.94)	10 (38.46)	25 (30.86)		
Watershed infarction, n (%)	16 (8.33)	14 (8.43)	2 (7.69)	14 (17.28)	1	0.031
CRP, mg/L	5.00 (1.97, 6.89)	5.00 (1.58, 6.18)	5.00 (3.06, 9.69)	5.00 (1.34, 7.00)	0.172	0.851
White blood cell, ×10 ⁹ /L	7.20 (5.57, 8.50)	6.90 (5.50, 8.40)	7.55 (6.20, 8.73)	7.50 (6.20, 9.30)	0.248	0.095
Fibrinogen, g/L	2.68 (2.21, 3.17)	2.65 (2.21, 3.10)	3.19 (2.59, 4.02)	2.62 (2.27, 3.17)	0.005	0.917
D-dimer, mg/L	0.73 (0.34, 1.77)	0.73 (0.34, 1.80)	0.72 (0.32, 1.37)	0.58 (0.31, 1.63)	0.680	0.583
Creatinine, μmol/L	77.00 (64.75, 91.00)	78.00 (64.25, 92.75)	71.00 (65.25, 85.75)	78.00 (62.00, 97.00)	0.215	0.810
Urea nitrogen, mmol/L	6.00 (5.01, 7.79)	5.94 (4.99, 7.75)	6.21 (5.36, 7.73)	6.19 (4.93, 7.91)	0.730	0.621
Glucose, mmol/L	6.50 (5.64, 8.61)	6.42 (5.61, 8.03)	7.19 (5.97, 9.91)	6.40 (5.39, 9.23)	0.061	0.680
Cystatin C, mg/L	1.06 (0.89, 1.27)	1.08 (0.89, 1.29)	1.01 (0.93, 1.19)	1.04 (0.94, 1.29)	0.371	0.932
Homocysteine, μmol/L	14.12 (11.12, 20.15)	14.24 (11.16, 19.93)	13.73 (10.83, 21.31)	13.86 (11.40, 18.31)	0.738	0.686
TG, mmol/L	1.16 (0.87, 1.54)	1.12 (0.86, 1.53)	1.36 (0.95, 1.59)	1.36 (0.91, 2.13)	0.288	0.058
TC, mmol/L	4.85 (4.20, 5.92)	4.78 (4.18, 5.81)	5.51 (4.65, 6.29)	4.97 (3.97, 5.91)	0.102	0.546
HDL, mmol/L	1.24 (1.07, 1.43)	1.23 (1.06, 1.41)	1.36 (1.14, 1.53)	1.19 (0.96, 1.35)	0.170	0.066
LDL, mmol/L	3.05 (2.54, 3.80)	3.02 (2.53, 3.75)	3.30 (2.77, 3.87)	2.92 (2.28, 3.68)	0.165	0.287
NLR	2.26 (1.56, 3.55)	2.01 (1.52, 3.13)	3.78 (2.87, 7.79)	2.25 (1.70, 3.85)	<0.001	0.452
PLR	114.81 (81.72, 160.15)	109.77 (78.93, 149.31)	155.32 (107.86, 254.44)	115.06 (86.58, 172.88)	0.001	0.801
LMR	3.99 (2.96, 5.18)	4.04 (3.20, 5.16)	3.54 (2.01, 5.04)	3.79 (2.86, 4.89)	0.069	0.384
Radiomics score	-2.13 (-3.07, -1.47)	-2.30 (-3.24, -1.57)	-1.10 (-1.82, -0.78)	-2.31 (-3.28, -1.38)	<0.001	0.883

Data are shown as median (interquartile range) or n (%).

CAD = coronary artery disease; CRP = C-reactive protein; DNT = door-to-needle time; HDL = high-density lipoprotein; LDL = low-density lipoprotein; LMR = lymphocyte-to-monocyte ratio; NIHSS = National Institutes of Health Stroke Scale; NLR = Neutrophil-to-lymphocyte ratio; OTA = onset-to-arrival; PLR = platelet-to-lymphocyte ratio; TC = total cholesterol; TG = triglyceride; TOAST = Trial of ORG 10172 in Acute Stroke Treatment criteria.

^a*p* Value: non-END vs END.

^b*p* Value training cohort vs validation cohort.

0.001), there were no significant differences in the other indicators between the END and non-END groups.

3.2. Radiomics feature analysis and radscore calculation

In this study, 1307 radiomics features were extracted from the data of each patient. A total of 310 radiomics features were found to be stable after screening using ICCs. Subsequently, a *t* test was used to select 105 radiomic features. Ultimately, the optimal regulation weight λ ($\lambda = 0.03$) for the LASSO algorithm was determined, and the seven most significant features with nonzero coefficients were

selected to build the radiomic signature (Fig. 3A, B). The equation was as follows: Radscore = -2.66 (constant) + coefficients × features. Fig. 3C shows the specific names and weights of the seven radiomics features. Fig. 3D, E depicts the radscore distribution in the training and validation cohorts. Patients with END had higher radscores than those in patients without END. In the training cohort, the median radscore values differed significantly between the END and non-END groups (-1.10 vs -2.30, $p < 0.001$). In the validation cohort, the median radscore of the END group was -0.81, which was significantly higher than that of the non-END group (-2.40, $p < 0.001$).

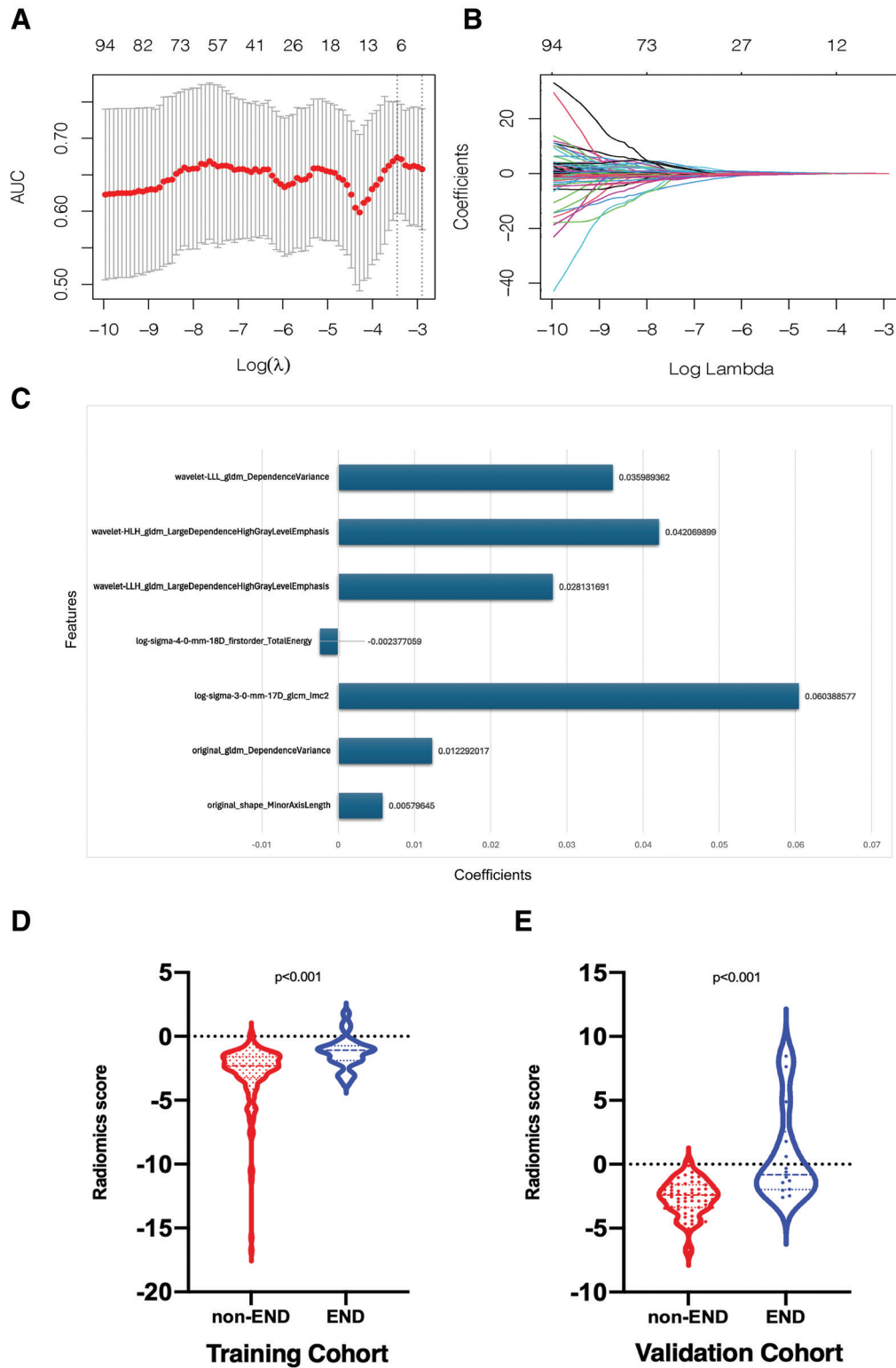


Fig. 3 LASSO feature selection and radiomics score calculation. A, The 5-fold cross-validation of the LASSO analysis was performed to determine the optimal lambda value. B, Regression coefficients of the LASSO analysis. C, Selected radiomic features and their corresponding coefficients. D and E, Radiomics score distribution of non-END and END groups in the training and validation cohorts. END = early neurological deterioration; LASSO = least absolute shrinkage and selection operator.

3.3. Logistic regression findings

In univariate logistic regression analysis, variables including NIHSS score, glucose, fibrinogen, NLR, and PLR demonstrated

statistically significant differences ($p < 0.05$), as shown in Table 2. Upon progression to multivariate logistic regression, NIHSS score and NLR exhibited significant differences.

Table 2
Univariate and multivariate regression findings

Variable	Univariate logistic regression		Multivariate logistic regression	
	OR (95% CI)	<i>p</i>	OR (95% CI)	<i>p</i>
NIHSS	1.25 (1.22-1.39)	<0.001	1.22 (1.08-1.37)	0.001
Glucose	1.15 (1.01-1.30)	0.032	-	-
Fibrinogen	1.93 (1.26-2.94)	0.002	-	-
NLR	1.46 (1.23-1.75)	<0.001	1.53 (1.14-2.05)	0.005
PLR	1.01 (1.00-1.01)	0.001	-	-

NIHSS = National Institutes of Health Stroke Scale; NLR = neutrophil-to-lymphocyte ratio; OR = odds ratio; PLR = platelet-to-lymphocyte ratio.

3.4. Clinical-radiomics nomogram establishment and evaluation

Based on the outcomes of the multivariate logistic regression analysis, a predictive clinical model was developed. The development of the clinical-radiomics nomogram integrated both the radiomics-derived score and pivotal patient-specific variables, including NIHSS and NLR, as depicted in Fig. 4A. For instance, when using the nomogram, a patient presenting with a radscore of 2 (equivalent to 100 points on the scale), an initial NIHSS score of 14 (assigned 15 points), and an NLR of 10 (corresponding to 15 points) would have an END probability exceeding 90%. In contrast, a score of 69.50 points, which is derived from a radscore of -6 (valued at 60 points), an NIHSS score of 6 (translated to 6.50 points), and an NLR of 2 (valued at 3 points), indicates an END probability of <10%. Fig. 4B, C shows the calibration plots for the clinical-radiomics nomogram representing the training and validation cohorts, respectively. The Hosmer-Lemeshow test, which is commonly used to assess the goodness-of-fit for logistic regression models, yielded a nonsignificant result ($p = 0.899$) for the training cohort, indicating favorable calibration. ROC analysis demonstrated that the clinical-radiomics model exhibited a modestly better performance than the radiomics and clinical models in distinguishing between non-END and END, with an AUC of 0.89 and a 95% CI ranging from 0.83 to 0.95 (Fig. 4D, Table 3). The clinical-radiomics model also exhibited favorable calibration and discrimination properties within the validation cohort, as evidenced by a nonsignificant Hosmer-Lemeshow goodness-of-fit test (Fig. 4C; $p = 0.825$) and an AUC of 0.95 (Fig. 4E; 95% CI, 0.90-0.99).

In addition, Table 3 shows the accuracies, sensitivities, specificities, PPV, and NPV for the radiomics, clinical, and clinical-radiomics models. The clinical-radiomics model demonstrated superior predictive performance compared with the radiomics model and clinical model. DCA demonstrated that the clinical-radiomics model possessed superior clinical utility, with greater net clinical benefits than that of the traditional clinical model (Fig. 4f).

4. DISCUSSION

In this study, we utilized an initial radiomic signature extracted from MRI images performed post-thrombolysis to forecast the likelihood of END. Our findings indicated a robust correlation between the radscore and the incidence of END following intravenous thrombolysis. The radscore was incorporated into a clinical nomogram model capable of predicting END probability in patients with stroke. The clinical-radiomics model exhibited adequate predictive precision for END and outperformed standalone clinical and radiomics models in terms of discriminatory power. Furthermore, the clinical application of this composite model was verified by DCA.

Occurring within the initial 24-hour period post-intravenous thrombolysis for stroke, END is a frequent event that significantly correlates with unfavorable outcomes within the subsequent three months.²⁰ The anticipation of END has emerged as a critical therapeutic aim in the acute ischemic stroke management paradigm, given its prevalence and profound impact on clinical results after intravenous thrombolysis.⁶ However, predicting END poses considerable clinical challenges. DWI, a frequently applied MRI technique for stroke assessment, offers rapid image acquisition facilitated by echo planar imaging and is less prone to motion artifacts when juxtaposed with traditional spin-echo imaging sequences.^{21,22} DWI has the necessary sensitivity to identify cerebral ischemia during the earliest stages of stroke onset.²³ Consequently, harnessing the image characteristics of DWI to expedite the pinpointing of END after intravenous thrombolysis is promising.

Radiomics is an advanced analytical technique for extracting significant quantitative features from medical images and serves as a robust tool for informing modern medical diagnostics and therapeutics.²⁴⁻²⁶ This approach has demonstrated superior precision in characterizing the heterogeneity of acute ischemic stroke lesions compared to that of standard imaging analysis methods.²⁷ In a study by Tang et al,¹⁶ a predictive model for recurrent stroke was developed using a radiomics nomogram in patients with symptomatic intracranial atherosclerotic stenosis, revealing the utility of radiomics features in forecasting recurrent strokes. Additionally, a novel deep learning model incorporating DWI and apparent diffusion coefficient (ADC) radiomic features was designed to determine stroke onset timing, potentially guiding decision-making regarding thrombolytic therapy for patients with unknown stroke onset time.²⁸ Oge et al²⁹ have indicated that radiomic assessments of ADC in the context of ischemic pontine lesions may serve as predictors for END. Their study involved an evaluation of patients presenting with isolated pontine infarcts who underwent MRI scans within a 48-hour window of symptom onset. The mean ADC value of the ischemic voxels in the affected area was determined and compared with that of the contralateral, nonischemic tissue, with findings indicating a notably reduced relative ADC value in patients who developed END.²⁹ However, the ADC threshold established in their analysis has not yet been externally validated. In our study, we conducted an initial exploration of the radiomics features derived from DWI of patients who underwent intravenous thrombolysis to predict END. The seven radiomic features utilized within the radiomics model effectively encapsulated the heterogeneity and complexity of cerebral infarcts. When assessing the significance of the features, our analysis revealed that texture-based features, such as GLCM and GLDM, were more important than shape and first-order statistical features. The most influential predictor, denoted as “glcm_Imc2,” evaluates the linkage between the probabilistic distributions associated with distinct pixel intensity ranges. Furthermore, GLDM quantifies the degree of similarity between neighboring voxels relative to a central voxel within a defined

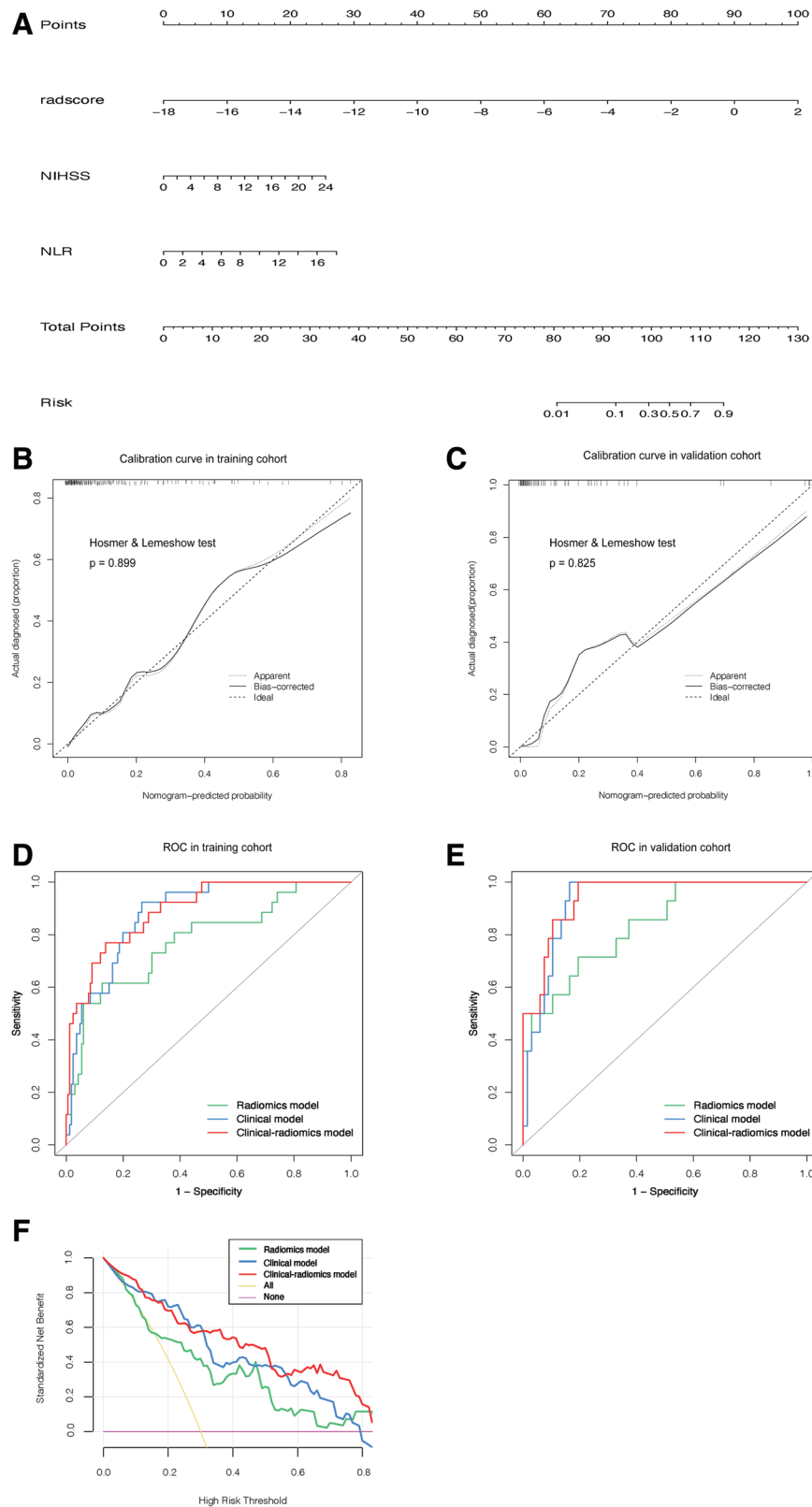


Fig. 4 The clinical-radiomics nomogram for predicting END. A, The nomogram, based on the clinical-radiomics prediction model, is designed to predict the risk of END. B and C, Calibration curves for the clinical-radiomics nomogram in the training and validation cohorts. D and E, ROC curves of the clinical model, radiomics model, and clinical-radiomics model in the training and validation cohorts. F, Decision curve analysis for the nomogram. The black line denotes the net benefit associated with the assumption that none of the patients with stroke will experience END. The purple line represents the net benefit under the assumption that all patients with stroke will develop END. The blue, green, and red lines represent the expected net benefit of predicting END using the clinical, radiomics, and clinical-radiomics models, respectively. END = early neurological deterioration; ROC = receiver operating characteristic.

Table 3
Performance of the predicative model

	Cohort	AUC (95% CI)	Accuracy	Sensitivity	Specificity	Pos. pred. value ^a	Neg. pred. value ^b
Radiomics model	Training cohort	0.78 (0.68-0.88)	0.84	0.62	0.87	0.43	0.94
	Validation cohort	0.84 (0.73-0.95)	0.79	0.71	0.81	0.44	0.93
Clinical model	Training cohort	0.88 (0.82-0.94)	0.76	0.89	0.74	0.34	0.98
	Validation cohort	0.93 (0.8-0.98)	0.86	1.00	0.84	0.56	1.00
Clinical-radiomics model	Training cohort	0.89 (0.83-0.95)	0.85	0.77	0.86	0.47	0.96
	Validation cohort	0.95 (0.90-0.99)	0.84	1.00	0.81	0.52	1.00

Balanced sensitivity and specificity at the cutoff yielding the largest Youden index value.

AUC = area under the receiver operating characteristic curve.

^aPositive predictive value.

^bNegative predictive value.

spatial context. The selected features demonstrated efficacy in predicting END, with promising results in both the training and validation cohorts.

Regarding clinical factors, numerous studies have focused on forecasting END in patients with stroke who have undergone intravenous thrombolysis. These studies have identified an array of factors linked to END, such as smoking, glucose, homocysteine, inflammatory cell ratios, NIHSS scores, and the use of antiplatelet therapy before thrombolysis.^{20,30,31} However, the findings from these studies were not uniformly aligned, possibly because of the heterogeneity present within the studies. In the present study, we deliberately excluded cases involving acute large vessel occlusions, as these patients are at a higher risk of END due to their potential for malignant edema or hemorrhagic transformation. Additionally, patients with END caused by hemorrhagic transformation following rt-PA administration were excluded. Therefore, clinical elements related to large vessel occlusion and hemorrhagic transformation were excluded from our analysis. The resulting patient group was relatively prevalent in clinical practice; however, the efficacy of pharmacological interventions within this group was typically constrained after the occurrence of END. Identifying the risk factors that contribute to END emergence within this cohort is of considerable importance. Our findings indicated that a higher baseline NIHSS score and NLR are predictive factors for END. In line with prior research, a positive correlation was found between the NIHSS score and the likelihood of END.³²⁻³⁴ Miyamoto et al³² noted that patients with an NIHSS score >8 at baseline are at an increased risk of END. This threshold was later incorporated into the WORSEN score, which is used to stratify patients according to their risk during the risk assessment process.³⁵ In our study, the median NIHSS score in the END group was 9. The role of NLR as a prominent predictor for END in patients with ischemic stroke undergoing thrombolysis has been acknowledged.^{30,36} Previous studies have reported that the NLR, as a potential novel biomarker, reflects the neuroinflammatory response, which is known to significantly affect the pathophysiological processes associated with ischemic stroke.^{37,38}

Although several predictive models for END after intravenous thrombolysis in ischemic stroke exist, they are primarily formulated using conventional clinical and imaging characteristics.^{30,33} In the current study, we enhanced these traditional predictive factors by incorporating features derived from radiomics. Although traditional clinical predictive models have demonstrated robust predictive power, our integrated clinical-radiomics model exhibited a slightly improved performance.

It is important to acknowledge the limitations of this study. First, the potential for selection bias exists in this retrospective, single-center study, which was compounded by the limited number of participants. Consequently, prospective multicenter

studies are needed to evaluate the generalizability of our predictive model across diverse patient cohorts. Additionally, the reliance on VOI segmentation in the current study may have introduced a degree of subjectivity, potentially affecting the precision of the radiomics analysis. The journey toward achieving an automated segmentation technique that rivals the accuracy and consistency of manual methods is lengthy.¹² Lastly, while DWI was utilized exclusively for the extraction of radiomics features in this study, acknowledging its heightened sensitivity in detecting early infarctions, there is a compelling argument for the advancement of multiparametric MRI-based methodologies. Such developments are expected to significantly enhance the predictive capabilities of radiomic analyses.

In conclusion, our DWI-based clinical-radiomics nomogram can effectively predict individual END in the early phase after intravenous thrombolysis, which may be helpful in the management of patients with acute ischemic stroke.

ACKNOWLEDGMENTS

This work was supported by the Good-Doctor Construction Project of the Yangpu District (grant number: 240201) and The Science and Technology Commission of the Yangpu District Fund (grant number: YPZQ202101).

REFERENCES

1. Collaborators GBDS. Global, regional, and national burden of stroke and its risk factors, 1990-2019: a systematic analysis for the Global Burden of Disease Study 2019. *Lancet Neurol* 2021;20:795-820.
2. Marko M, Posekany A, Szabo S, Scharer S, Kiechl S, Knoflach M, et al; Austrian Stroke Unit Registry Collaborators. Trends of r-tPA (Recombinant Tissue-Type Plasminogen Activator) treatment and treatment-influencing factors in acute ischemic stroke. *Stroke* 2020;51:1240-7.
3. Thiebaut AM, Gauberti M, Ali C, Martinez De Lizarrondo S, Vivien D, Yepes M, et al. The role of plasminogen activators in stroke treatment: fibrinolysis and beyond. *Lancet Neurol* 2018;17:1121-32.
4. Seners P, Turc G, Oppenheim C, Baron JC. Incidence, causes and predictors of neurological deterioration occurring within 24 h following acute ischaemic stroke: a systematic review with pathophysiological implications. *J Neurol Neurosurg Psychiatry* 2015;86:87-94.
5. Yu WM, Abdul-Rahim AH, Cameron AC, Korv J, Sevcik P, Toni D, et al; SITS Scientific Committee*. The incidence and associated factors of early neurological deterioration after thrombolysis: results from SITS registry. *Stroke* 2020;51:2705-14.
6. Mitsias PD. Early neurological deterioration after intravenous thrombolysis: still no end in sight in the quest for understanding END. *Stroke* 2020;51:2615-7.
7. Zhang Y, Wang J, Ma Z, Mu G, Liang D, Li Y, et al. Prospective pilot study of tirofiban in progressive stroke after intravenous thrombolysis. *Front Neurol* 2022;13:982684.

8. Seners P, Turc G, Tisserand M, Legrand L, Labeyrie MA, Calvet D, et al. Unexplained early neurological deterioration after intravenous thrombolysis: incidence, predictors, and associated factors. *Stroke* 2014;45:2004–9.
9. Arenillas JF, Rovira A, Molina CA, Grive E, Montaner J, Alvarez-Sabin J. Prediction of early neurological deterioration using diffusion- and perfusion-weighted imaging in hyperacute middle cerebral artery ischemic stroke. *Stroke* 2002;33:2197–203.
10. Shi Z, Zhu C, Degnan AJ, Tian X, Li J, Chen L, et al. Identification of high-risk plaque features in intracranial atherosclerosis: initial experience using a radiomic approach. *Eur Radiol* 2018;28:3912–21.
11. Quan G, Ban R, Ren JL, Liu Y, Wang W, Dai S, et al. FLAIR and ADC image-based radiomics features as predictive biomarkers of unfavorable outcome in patients with acute ischemic stroke. *Front Neurosci* 2021;15:730879.
12. Chen X, Li Y, Zhou Y, Yang Y, Yang J, Pang P, et al. CT-based radiomics for differentiating intracranial contrast extravasation from intraparenchymal haemorrhage after mechanical thrombectomy. *Eur Radiol* 2022;32:4771–9.
13. Jia X, Zhai Y, Song D, Wang Y, Wei S, Yang F, et al. A Multiparametric MRI-based radiomics nomogram for preoperative prediction of survival stratification in glioblastoma patients with standard treatment. *Front Oncol* 2022;12:758622.
14. Limkin EJ, Sun R, Derclé L, Zacharaki EI, Robert C, Reuze S, et al. Promises and challenges for the implementation of computational medical imaging (radiomics) in oncology. *Ann Oncol* 2017;28:1191–206.
15. Tang TY, Jiao Y, Cui Y, Zhao DL, Zhang Y, Wang Z, et al. Penumbra-based radiomics signature as prognostic biomarkers for thrombolysis of acute ischemic stroke patients: a multicenter cohort study. *J Neurol* 2020;267:1454–63.
16. Tang M, Gao J, Ma N, Yan X, Zhang X, Hu J, et al. Radiomics nomogram for predicting stroke recurrence in symptomatic intracranial atherosclerotic stenosis. *Front Neurosci* 2022;16:851353.
17. Egger J, Kapur T, Fedorov A, Pieper S, Miller JV, Veeraraghavan H, et al. GBM volumetry using the 3D Slicer medical image computing platform. *Sci Rep* 2013;3:1364.
18. Koo TK, Li MY. A guideline of selecting and reporting intraclass correlation coefficients for reliability research. *J Chiropr Med* 2016;15:155–63.
19. Hughes G. Youden's index and the weight of evidence. *Methods Inf Med* 2015;54:198–9.
20. Che F, Wang A, Ju Y, Ding Y, Duan H, Geng X, et al. Early neurological deterioration in acute ischemic stroke patients after intravenous thrombolysis with alteplase predicts poor 3-month functional prognosis - data from the Thrombolysis Implementation and Monitor of Acute Ischemic Stroke in China (TIMS-China). *BMC Neurol* 2022;22:212.
21. Kim BJ, Kang HG, Kim HJ, Ahn SH, Kim NY, Warach S, et al. Magnetic resonance imaging in acute ischemic stroke treatment. *J Stroke* 2014;16:131–45.
22. Lin J, Li X, Wu G, Chen X, Weng Y, Wang H, et al. White matter high signals interfere with noncontrast computed tomography in the early identification of cerebral infarction. *Cerebrovasc Dis* 2020;49:135–43.
23. Nagaraja N. Diffusion weighted imaging in acute ischemic stroke: a review of its interpretation pitfalls and advanced diffusion imaging application. *J Neurol Sci* 2021;425:117435.
24. Lambin P, Leijenaar RTH, Deist TM, Peerlings J, de Jong EEC, van Timmeren J, et al. Radiomics: the bridge between medical imaging and personalized medicine. *Nat Rev Clin Oncol* 2017;14:749–62.
25. Lambin P, Rios-Velazquez E, Leijenaar R, Carvalho S, van Stiphout RG, Granton P, et al. Radiomics: extracting more information from medical images using advanced feature analysis. *Eur J Cancer* 2012;48:441–6.
26. Gillies RJ, Kinahan PE, Hricak H. Radiomics: images are more than pictures, they are data. *Radiology* 2016;278:563–77.
27. Wen X, Li Y, He X, Xu Y, Shu Z, Hu X, et al. Prediction of malignant acute middle cerebral artery infarction via computed tomography radiomics. *Front Neurosci* 2020;14:708.
28. Zhang YQ, Liu AF, Man FY, Zhang YY, Li C, Liu YE, et al. MRI radiomic features-based machine learning approach to classify ischemic stroke onset time. *J Neurol* 2022;269:350–60.
29. Oge DD, Topcuoglu MA, Arsava EM. Apparent diffusion coefficient signature of ischemic tissue predicts neurological progression in isolated pontine infarcts. *Eur Stroke J* 2022;7:66–70.
30. Luo B, Yuan M, Kuang W, Wang Y, Chen L, Zhang Y, et al. A novel nomogram predicting early neurological deterioration after intravenous thrombolysis for acute ischemic stroke. *Heliyon* 2024;10:e23341.
31. Yang H, Lv Z, Wang W, Wang Y, Chen J, Wang Z. Machine learning models for predicting early neurological deterioration and risk classification of acute ischemic stroke. *Clin Appl Thromb Hemost* 2023;29:10760296231221738.
32. Miyamoto N, Tanaka Y, Ueno Y, Kawamura M, Shimada Y, Tanaka R, et al. Demographic, clinical, and radiologic predictors of neurologic deterioration in patients with acute ischemic stroke. *J Stroke Cerebrovasc Dis* 2013;22:205–10.
33. Jin H, Bi R, Zhou Y, Xiao Q, Li M, Sun S, et al. CNS-LAND score: predicting early neurological deterioration after intravenous thrombolysis based on systemic responses and injury. *Front Neurol* 2023;14:1266526.
34. Jin M, Peng Q, Wang Y. Post-thrombolysis early neurological deterioration occurs with or without hemorrhagic transformation in acute cerebral infarction: risk factors, prediction model and prognosis. *Heliyon* 2023;9:e15620.
35. Miyamoto N, Tanaka R, Ueno Y, Watanabe M, Kurita N, Hira K, et al. Analysis of the usefulness of the WORSEN score for predicting the deterioration of acute ischemic stroke. *J Stroke Cerebrovasc Dis* 2017;26:2834–9.
36. Gong P, Liu Y, Gong Y, Chen G, Zhang X, Wang S, et al. The association of neutrophil to lymphocyte ratio, platelet to lymphocyte ratio, and lymphocyte to monocyte ratio with post-thrombolysis early neurological outcomes in patients with acute ischemic stroke. *J Neuroinflammation* 2021;18:51.
37. Zhu B, Pan Y, Jing J, Meng X, Zhao X, Liu L, et al; CHANCE Investigators. Neutrophil counts, neutrophil ratio, and new stroke in minor ischemic stroke or TIA. *Neurology* 2018;90:e1870–8.
38. Parikh NS, Merkler AE, Iadecola C. Inflammation, autoimmunity, infection, and stroke: epidemiology and lessons from therapeutic intervention. *Stroke* 2020;51:711–8.